Elucidating Secondary Metal Cation Effects on Nickel Olefin Polymerization Catalysts

Thi V. Tran, Lucas J. Karas, Judy I. Wu, Loi H. Do*

Department of Chemistry, University of Houston, 4800 Calhoun Rd., Houston, Texas, 77204, United States

Keywords: olefin polymerization, coordination insertion, nickel catalysts, cation tuning, polyethylene

ABSTRACT: Secondary metal cations, such as alkali and transition metal ions, have been shown to enhance the catalytic performance of nickel and palladium olefin polymerization catalysts. Their beneficial effects can manifest in different ways, such as increasing rates of polymerization, altering polymer microstructures, enhancing catalyst thermal stability, or a combination of these effects. We have systematically quantified secondary metal ion influences on nickel phenoxyphosphine polyethylene glycol (PEG) complexes. We demonstrate that cation-tuning could readily achieve three-dimensional structures and electronic environments that are not easily accessible through conventional ligand-tuning. This study led to the development of extremely active ethylene polymerization catalysts. For example, the nickel-lithium complex gave activity and turnover number as high as 7.0×10^4 kg PE/mol Ni·h and 2.5×10^6 mol ethylene/mol Ni, respectively and the nickel-cesium complex showed unusual thermal stability up to 90 °C (activity = 2.3×10^4 kg/mol·h, turnover number = ~4.1×10^5 mol ethylene/mol Ni, M_n = 1.6×10^4 g/mol). We provide both experimental and computational data showing that secondary metals impact the relative stability of *cis* and *trans* isomers, which is a phenomenon not shown previously. Unlike in our earlier work, which was limited by poor nuclearity control and/or secondary metals that were too far from the catalyst center, the nickel phenoxyphosphine-PEG complex is an ideal platform for future studies of cation-controlled polymerization.

Introduction

Our society's long-standing fascination with polyethylene stems in part from the low cost of ethylene and the broad range of materials properties attainable by tailoring its microstructure and composition.[1] The discovery in the 1990s that Ni and Pd diimine complexes are excellent catalysts for olefin polymerization[2,3] led to several decades of research to create new variants with expanded capabilities,[4-12] such as those that could produce ultra high molecular weight polymers[13-15] or incorporate high percentages of polar olefins.[16-18] Traditional polymer synthesis typically follows the "one catalyst one material" paradigm, in which a single catalyst produces a single type of polymer structure (Scheme 1, left). This strategy is limiting because it does not allow for user control of the polymerization process.[19] For example, conventional catalysts are incapable of generating block copolymers from a single monomer pool or forming gradient polymers without external control.[20] For practical applications, catalysts that could easily produce different polymer structures *on demand* would make customized polymer synthesis more accessible to non-chemists, who might lack the expertise to create derivatives of the coordination catalyst. Furthermore, although exhaustive work has been invested in developing large libraries of olefin polymerization catalysts, there are limits to what molecular structures could be reasonably synthesized even by skilled chemists. Thus, significant gaps in the polyolefins space still exist, which represents exciting areas for further research and development in polymerization catalysis.

Toward the goal of realizing the "one catalyst many materials" concept,[19] researchers have pursued innovative approaches to control the polymerization process. One such strategy relies on varying the reaction parameters and/or components. For example, Arriola and coworkers took advantage of chain transfer agents to shuttle polymer chains between distinct Hf and Zr catalysts to produce olefin block copolymers with unique elastomeric properties.[21] The amount of chain transfer agents used relative to ethylene was varied to obtain materials with different crystallinity and transparency. Coates and coworkers demonstrated that living Ni diimine catalysts could be subjected to alternating changes in temperature and pressure to synthesize tetrablock polymers directly from ethylene.[22] These tetrablock materials enhanced the toughness of low-density and high-density polyethylene blends at ratios in which they would otherwise be phase separated. Finally, Coates, Fors, and coworkers used metered catalyst addition to control the shape of polyethylene molecular weight distributions.[23] This study showed that molecular weight distribution shape affects a material's viscosity but not tensile strength.

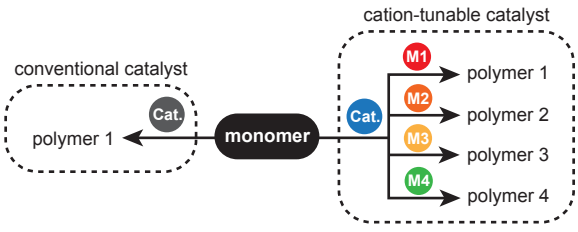

Scheme 1. Comparison of conventional versus cation-tunable polymerization catalysts.

An alternative strategy that has emerged in recent years is the application of tunable catalysts in polymerization.[24-30] Tunable catalysts are complexes that could be toggled between different reactivity states in response to external stimuli.[31] For example, catalysts bearing ferrocene groups[32-34] or redox active ligands[35] were shown to exhibit different olefin polymerization rates and polymer branching density upon the addition of chemical reductants or oxidants. Redox switching is operationally simple and does not require changes in reaction conditions. Tunable catalysts that rely on light as photo-triggers are also being developed to prepare polyolefins[36] and related hybrid materials.[37,38]

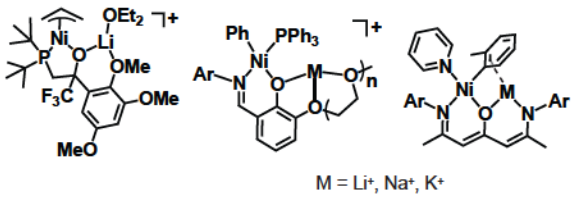

Chart 1. Representative examples of nickel-alkali complexes studied in ethylene polymerization catalysis. The examples shown were reported by Brookhart/Johnson (left),[39] Do (middle),[40,41] and Tonks (right)[42] groups.

Our laboratory has been interested in a subset of tunable catalysts that take advantage of secondary metal binding.[43] Unlike redox- and light-tuning that typically toggles between 2-3 catalyst states, cation-tuning could potentially access a wider range because M^{n+} can differ in size, charge, Lewis acidity, redox activity, and other characteristics. In 2003, Johnson, Brookhart, and coworkers were the first to report that external cations were beneficial to olefin polymerization (Chart 1, left).[39] They found that addition of Li^+ to nickel alkoxyphosphine catalysts provided a significant boost in catalyst activity. Other investigators have also taken advantage of secondary metals in coordination catalyst designs. For example, Tonks and coworkers demonstrated that alkali ions could influence the tautomeric structure of nickel β-oxo-δ-diimine catalysts (Chart 1, right).[42] Jordan and coworkers showed that lithium[44-47] and zinc[48] ions could induce the spontaneous self-assembly of catalyst cages that exhibited unique polymerization behavior. These examples illustrate beautifully the diverse chemistry that could be leveraged by integrating secondary metals into polymerization systems.

Because of their highly tunable nature, cation-tunable catalysts are ideal platforms to test the feasibility of a user-customizable polymer synthesis approach, where different polymer structures could be obtained by pairing the catalyst with different secondary metals (Scheme 1, right).[43] Toward this goal, our research group has developed several catalyst prototypes supported by ligands featuring polyethylene glycol (PEG) side chains (Chart 1, middle). They include complexes based on phenoxyimine,[40,41] phosphine phosphonate ester,[49,50] and phenoxyphosphine.[51] The PEG groups are integral to our catalyst design because they provide well-defined secondary metal binding pockets for a variety of metal cations. It has also been used successfully as a ligand substituent by Chen and coworkers.[52] In our ethylene polymerization studies, we observed that combining secondary metals with either Ni or Pd catalyst often gave favorable polymerization results, such as rate acceleration or changes to the polymer architecture. Some of the most confounding questions that arose out of our investigations were: What were the roles of the secondary metals in polymerization? Are cation effects simply manifestations of steric and electronic effects? To investigate these fundamentally important questions, we have undertaken a systematic study to determine how binding of alkali ions to nickel phenoxyphosphine-PEG complexes impacts their catalyst properties and polymerization tendencies. We quantified secondary metal cation effects using a variety of spectroscopic and analytical tools, and applied computational methods to explore possible catalyst structures. We discovered that our nickel-alkali complexes are among some of the most productive late transition metal coordination catalysts reported to date and the identity of the alkali ions strongly influences the polymerization outcome. Our results suggest that steric and electronic parameters are useful descriptors of metal cation effects but that other factors such as coordination interactions could have possible roles in catalysis. Importantly, we show that our Ni phenoxyphosphine-PEG construct has overcome previous catalyst design issues, which allowed us to extract useful lessons for future developments in cation-controlled catalysis.

Results and Discussion

Catalyst Selection and Secondary Metal Binding. One of the major challenges in creating cation-tunable catalysts is coupling secondary metal binding with programmed changes in form and function. Although we showed that pendant metal binding sites could be installed in different olefin polymerization catalyst platforms, we had encountered various challenges. For example, we found that Ni phenoxyimine-PEG complexes could dimerize in the presence of substoichiometric amounts of alkali ions,[40] Ni triazolecarboxamidate-pyridine complexes formed ill-defined species upon addition of zinc ions,[53] and Ni phosphine phosphonate-PEG complexes gave heterobimetallic structures that have non-interacting nickel and alkali centers.[50] In contrast, the Ni phenoxyphosphine-PEG complexes (**Ni3**) gave well-behaved molecular species in the presence of sodium salts.[51] Because of these encouraging results, we focused our current investigations on **Ni3** and its nickel-alkali derivatives (**Ni3**-M, where M = Li^+, Na^+, K^+, and Cs^+). As representative examples of conventional mononickel catalysts,[54-56] we also studied **Ni1**[54] and **Ni2**[51] bearing pentafluorophenyl and *tert*-butyl groups, respectively, at the *ortho* positions of their phenolate moieties (Scheme 2).

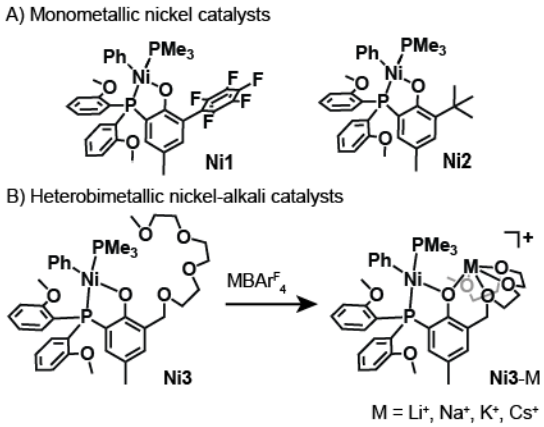

Scheme 2. Monometallic nickel (conventional) and heterobimetallic nickel-alkali complexes used in this study.

We had shown previously that conventional nickel phenoxyphosphine complexes lacking *ortho* PEG groups do not bind secondary metals to an appreciable extent.[51] In contrast, **Ni3** produced discrete 1:1 nickel-sodium species in solution and the solid state. To investigate whether **Ni3** could form adducts with other alkali ions, we performed metal ion titrations using UV-visible absorption spectroscopy. We observed that addition of 1.0 equiv. of $MBAr^F_4$ (M = Li^+, Na^+, K^+, Cs^+; $BAr^F_4{}^-$ = tetrakis(3,5-bis(trifluoromethyl)phenyl)borate) to **Ni3** in Et_2O led to clear optical changes with the appearance of multiple isosbestic points, suggesting of **Ni3** and M^+ binding (Figure S1). For example, when aliquots of $LiBAr^F_4$ were combined with **Ni3**, the band at 372 nm decreased concomitant with an increase at 326 nm (Figure 1A). Interestingly, when LiOTf (OTf^- = triflate anion) was used instead of $LiBAr^F_4$, the spectra of **Ni3** only showed minor changes (Figure S1E). Presumably, the more coordinating triflate can compete with **Ni3** for alkali ion binding whereas the less coordinating tetraarylborate cannot. As expected, the spectra of the nickel-alkali species all showed slightly different λ_{max} values, consistently with the different electronic effects of M^+ on **Ni3**.

To ascertain the optimal nickel:alkali binding stoichiometry in solution, the method of continuous variation was employed. Although the polymerization studies below were conducted in toluene, Et_2O was used for these studies because polar solvents are needed to dissolve high concentrations of alkali salts. As shown in Figure 1B, the Job plots for **Ni3** + M^+ all gave peak maxima at χ_{Ni} = 0.5, which is indicative of 1:1 nickel to alkali ion binding. Their curvatures suggest that the affinities of **Ni3** for alkali metals are approximately in the order $Li^+ > Na^+ \sim K^+ > Cs^+$.[57] However, further binding studies are needed to confirm this order. These results are consistent with other studies showing that the PEG group has different association constants with different metal ions.[40,58,59]

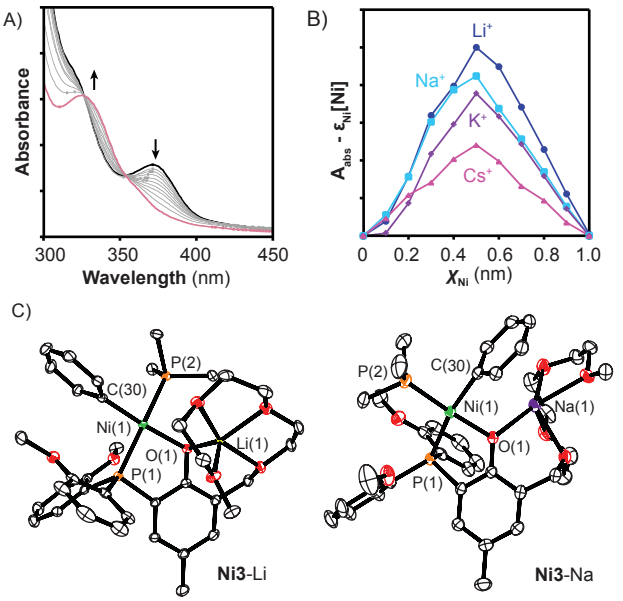

Figure 1. A) UV-vis absorbance spectra of **Ni3** (black trace, 100 μM in Et_2O) after the addition of 1.0 equiv. of $LiBAr^F_4$ (red trace); B) Job plots obtained from binding studies of **Ni3** + $MBAr^F_4{}^-$; C) Molecular structures of **Ni3**-Li and **Ni3**-Na (ORTEP view, displacement ellipsoids drawn at 50% probability). Hydrogen atoms and $BAr^F_4{}^-$ have been omitted for clarity.

Characterization of Nickel-Alkali Complexes. To gain insight into the structures of the heterobimetallic species, single crystals of the **Ni3**-M complexes were grown and analyzed by X-ray crystallography. Their nickel centers all showed square planar geometries, although **Ni3**-Li (Figure 1C), **Ni3**-K (Figure S37), and **Ni3**-Cs (Figure S38) displayed *cis* arrangements of their P(1) and C(30) donors (isomer **A**) whereas **Ni3**-Na displayed a *trans* arrangement (isomer **B**).[51] Isomer **A** is typically more thermodynamically favored because its strongest σ-donors, P(1) and C(30), prefer being *cis* to each other rather than *trans* to avoid sharing the same nickel *d*-orbital.[60,61] A distinct feature of the solid state structure of **Ni3**-Na is the close contact between Na^+ and the nickel-coordinated phenyl ring (Na(1)–C(30) = 2.98 Å, Na(1)–C(31) = 3.04 Å),[62] which suggests that metal-π interactions could provide enough stabilization energy to overcome the *trans* influence (vide infra). This type of alkali-π interactions has been observed in the solid state by us[40,51] and others.[42]

The coordination spheres of the alkali metals in **Ni3**-M are slightly different due to variations in their ionic radii and coordination numbers. For example, the Li^+ ion in **Ni3**-Li is ligated by the phenolate oxygen donor and four ether oxygen atoms from PEG (Figure 1C). Complex **Ni3**-Na also has an oxygen-rich environment around Na^+, except for an additional sodium-π interaction as described above.[51] Interestingly, the alkali ions in **Ni3**-K (Figure S37) and **Ni3**-Cs (Figure S38) are surrounded by five oxygen donors as well tetrahydrofuran and benzene molecules, respectively. Although the presence of external adducts may be artifacts of the crystallization solvents used, the increasing coordination numbers observed going from $Li^+ \rightarrow Na^+ \rightarrow K^+ \rightarrow Cs^+$ is consistent with the atomic size of the secondary ions.[63]

Table 1. Comparison of Atomic Distances[a]

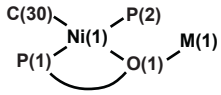

	Ni1′[b,c]	**Ni2**[c]	**Ni3**-Li	**Ni3**-Na[c]	**Ni3**-K	**Ni3**-Cs
Isomer	-	A	A	B	A	A
Ni(1)–P(1)	2.176	2.186	2.194	2.221	2.203	2.167
Ni(1)–O(1)	1.938	1.913	1.936	1.936	1.936	1.921
Ni(1)–C(30)	-	1.895	1.889	1.916	1.899	1.902
Ni(1)–P(2)	-	2.186	2.192	2.135	2.182	2.192
M(1)–O(1)	-	-	1.933	2.313	2.592	3.121
Ni(1)–M(1)	-	-	3.208	3.486	3.899	3.831

[a]All atomic distances are given in angstroms. [b]Complex **Ni1′** does not have phenyl and trimethylphosphine ligands coordinated to nickel. [c]X-ray structures previously reported.

Next, we compared the bond metrics of **Ni3**-M to those of their mononickel counterparts (Table 1). Although the X-ray structure of **Ni3** could not be obtained because the complex is not crystalline, the structures of **Ni1′**[54] (Chart S1) and **Ni2**[51] were readily available. Complex **Ni1′** is supported by a phe-

noxyphosphine donor similar to that in **Ni1**, except that it is also chelated by cyclooctene instead of phenyl and trimethylphosphine donors.

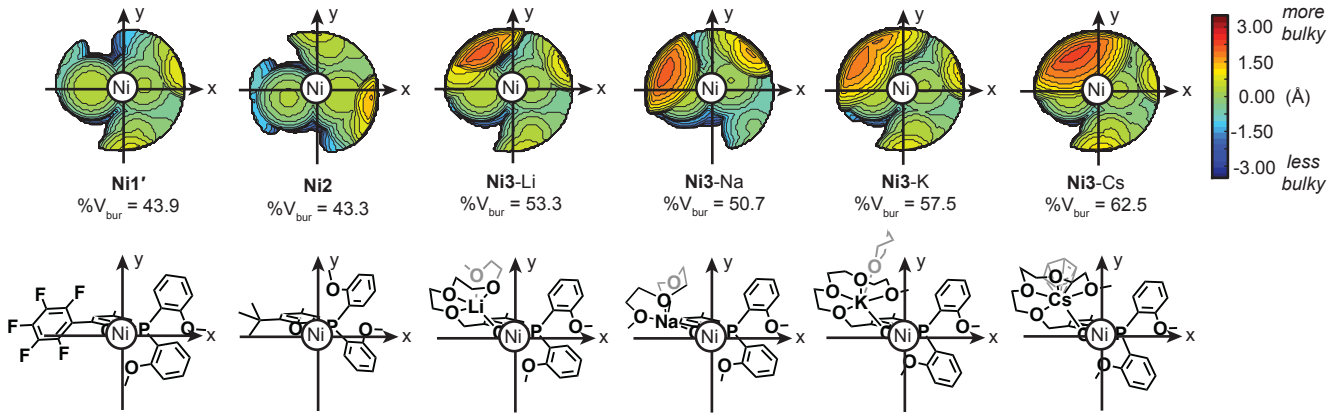

Figure 2. Top: topographic steric maps of the nickel complexes calculated from their X-ray structures using SambVca 2.1. Only the phenoxyphosphine ligands were considered in the calculation of $\%V_{bur}$. The nickel atom was set as the center of the coordination sphere, the nickel square plane defined the *xz*-plane, and the z-axis bisects the P(1)–Ni(1)–O(1) angle. The crystallographic data for **Ni1′**, **Ni2**, and **Ni3**-Na were obtained from published data. Bottom: chemical structures corresponding to the steric maps above shown in the same front view perspective.

Complex **Ni2** has the standard formula [Ni(Ph)(PMe_3)(L)] (where L = compound **4**, see Scheme S1) and was crystallized in the isomer **A** form. Comparison of the atomic distances in the nickel complexes showed only slight differences. For example, the Ni(1)–O(1) length in **Ni3**-M was about 1.92-1.94 Å whereas that in **Ni2** was 1.91 Å. Variations in the other bond lengths between **Ni3**-M and **Ni2** were typically less than 0.05 Å. As expected, the most pronounced differences are in the M(1)–O(1) separations, which ranged from 1.93 to 3.12 Å going from **Ni3**-Li to **Ni3**-Cs in accordance with the increasing ionic radii of M^+.[63] Surprisingly, the Ni(1)–K(1) distance is slightly longer than that of Ni(1)–Cs(1) (3.90 vs. 3.83 Å, respectively), which might be due to effects of their different solvent adducts (e.g., differences in electronic donation from THF vs. toluene).

Having crystallographic characterization of the complete **Ni3**-M series allowed us to compare the steric congestion in their active site pockets. Although a variety of descriptors have been used to define steric bulk, we prefer percentage of buried volume ($\%V_{bur}$) because it could be applied to many catalyst structures and is simple to determine using the SambVca 2.1 program.[64,65] In addition, $\%V_{bur}$ values have been reported for other olefin polymerization catalysts so direct comparisons could be made with those complexes.[17,18,66] In our calculations, $\%V_{bur}$ only took into account the fraction of the first coordination sphere occupied by the phenoxyphosphine-PEG ligand + alkali ion. As shown in the topographic steric maps in Figure 2, the nickel-alkali complexes displayed $\%V_{bur}$ values in the order **Ni3**-Na (50.7) < **Ni3**-Li (53.3) < **Ni3**-K (57.5) < **Ni3**-Cs (62.5). Although the $\%V_{bur}$ for **Ni3**-Li does not seem to follow the atomic size trend (ionic radii = 76 pm for Li^+, 102 pm for Na^+, 138 pm for K^+, and 167 pm Cs^+),[63] we attributed this apparent discrepancy to shorter alkali-PEG bonds in **Ni3**-Li compared to those in **Ni3**-Na, which brought the pendant lithium-PEG unit closer to Ni and consequently, led to enhanced $\%V_{bur}$. Interestingly, when the **Ni3**-M structures were viewed from the side (looking down the *x*-axis, Figure S11), the alkali-PEG groups afforded varying amount of axial site coverage. Specifically, the Li^+ and Cs^+ cations appeared to provide greater steric protection than Na^+ and K^+. However, the southwest quadrants (when viewed down the *z*-axis, front view) of the **Ni3**-M complexes are open to the external environment, suggesting that this space could be protected better in future catalyst designs.

The $\%V_{bur}$ for **Ni1′** and **Ni2** were determined to be 43.9 and 43.3, respectively (Figure 2). These values are similar to those reported for related palladium *P,O*-ligated polymerization catalysts ($\%V_{bur}$ = 41.5–49.6[17] and 45.3-47.8[67]). Although much higher $\%V_{bur}$ values could be achieved using symmetric diimine ligands with ultra bulky groups (e.g., up to 87.6% buried volume),[66] many asymmetric ligand platforms such as phosphine sulfonates could only be bulked up on the phosphine side.[8] Comparison of our $\%V_{bur}$ data revealed the alkali-PEG units could enhance steric protection by up to ~19% in volume compared to that by common ligand substituents such as pentafluorophenyl (**Ni1′**) or *tert*-butyl (**Ni2**) groups. In addition, **Ni1′** and **Ni2** are devoid of steric protection at their axial positions (side view, Figure S10), which could prevent efficient polymerization and reduce thermal stability.[4] These results clearly indicate the **Ni3**-M structures are unique and cation binding as a way of fine-tuning steric bulk could be advantageous over conventional methods that rely on synthetic ligand modifications.

Table 2. Electrochemical Data for Nickel Complexes[a]

Complex	***E*** (*vs.* Fc/Fc^+, mV)	**Δ*E*** (*cf.* **Ni3**, mV)
Ni1	26	+76
Ni2	-49	+1
Ni3	-50	0
Ni3-Li	56	+106
Ni3-Na	-14	+36
Ni3-K	-16	+34
Ni3-Cs	-24	+26

[a]The cyclic voltammograms of the nickel complexes were measured in THF with 0.09 M nBu$_4$NBPh$_4$ supporting electrolyte and 200 mV/s scan rate. The oxidation potentials were references to ferrocene/ferrocenium.

Next, we evaluated how secondary metal binding impacts the nickel electron density using cyclic voltammetry (Table 2, Figure S19). The heterobimetallic species were formed in situ by combining **Ni3** with 1 equiv. of $MBAr^F_4$ in THF with nBu$_4$NBPh$_4$ as the supporting electrolyte. Both mononickel and nickel-alkali complexes showed irreversible anodic waves, which were tentatively ascribed to the one-electron oxidation of Ni(II) to Ni(III).[68,69] The oxidation peak for **Ni3** occurred at -50 mV (vs. Fc/Fc^+) and was used as reference for comparison with the other complexes. Complex **Ni2** with a slightly electron-donating *tert*-butyl group had a similar oxidation potential as that of **Ni3** (E = -49 mV), whereas **Ni1** with an electron-withdrawing pentafluorophenyl group oxidized at a more positive potential (E = +26 mV). The presence of secondary alkali ions shifted the anodic peak in accordance to their relative Lewis acid strength,[70] giving E in the order **Ni3**-Li (+56 mV) > **Ni3**-Na (-14 mV) ~ **Ni3**-K (-16 mV) > **Ni3**-Cs (-24 mV). Interestingly, the ΔE of **Ni3**-Li (vs. **Ni3**) is larger than that of **Ni1** (+106 mV vs. +76 mV, respectively), which suggests Li^+ binding reduces the electron density of Ni to a greater extent than electronic induction by pentafluorophenyl substituents.

On the basis of their structural and electronic features, **Ni3**-M complexes are clearly distinct from conventional nickel phenoxyphosphine complexes (e.g., **Ni1** and **Ni2**). Because the alkali-PEG units in **Ni3**-M vary in shape and size, depending on the identity of M^+ and possible solvent interactions, they have different space filling capacity within the nickel coordination sphere (Figure 2). At the same time, the alkali ions increase the effective charge of the nickel centers, which provides a convenient way to tune their electron density and electrophilicity. We will discuss in the last section that pendant metal cations are also capable of secondary coordination interactions, which could impact the relative stability of *cis* and *trans* isomers.

Table 3. Ethylene Polymerization by Nickel Catalysts at Various Temperatures[a]

Entry	Catalyst	Salt	Temp. (°C)	Polymer Yield (g)	Activity (kg/mol·h)	Branches[b] (/1000 C)	M_n[c] ($\times 10^3$)	M_w/M_n[c]
1	**Ni1**	none	30	0.77	1500	9	3.06	2.1
2	**Ni2**	none	30	1.32	2600	15	5.20	1.9
3	**Ni3**	none	30	trace	0	–	–	–
4[d]	**Ni3**	Li^+	30	3.53	35000	12	40.10	1.3
5	**Ni3**	Na^+	30	9.07	18000	27	1.72	1.4
6	**Ni3**	K^+	30	1.46	2900	25	4.53	1.6
7	**Ni3**	Cs^+	30	0.18	360	9	33.93	1.5
8[d]	**Ni3**	Li^+	50	3.84	38000	7	12.10	1.3
9	**Ni3**	Na^+	50	6.52	13000	30	1.60	1.2
10	**Ni3**	K^+	50	2.73	5500	9	11.50	1.5
11	**Ni3**	Cs^+	50	0.72	1400	8	34.98	1.3
12[d]	**Ni3**	Li^+	70	1.82	18000	10	6.20	1.3
13	**Ni3**	Na^+	70	4.61	9200	27	1.03	1.4
14[e]	**Ni3**	K^+	70	2.89	12000	27	1.39	1.3
15[e]	**Ni3**	Cs^+	70	9.12	36000	9	15.12	1.7
16	**Ni1**	none	90	10.3	21000	15	0.97	3.7
17	**Ni2**	none	90	12.8	26000	12	1.46	3.4
18[d]	**Ni3**	Li^+	90	1.31	13000	17	2.09	2.2
19	**Ni3**	Na^+	90	2.41	4800	30	0.86	1.5
20[e]	**Ni3**	K^+	90	2.49	10000	29	1.06	1.6
21[e]	**Ni3**	Cs^+	90	5.73	23000	10	15.74	1.4

[a]Polymerization conditions: Ni catalyst (0.5 μmol), $MBAr^F_4$ (1 μmol, if any), $Ni(COD)_2$ (4 μmol), ethylene (450 psi), 100 mL toluene, 1h. Temperature was controlled by manual external cooling when necessary to ensure the reaction temperature does not exceed greater than 5 °C from the starting temperature. Reported yields are the average of 2-3 runs and standard deviations are less than 10%. [b]The total number of branches per 1000 carbons was determined by ^{1}H NMR spectroscopy. [c]Determined by GPC in trichlorobenzene at 140 °C. [d]**Ni3** (0.1 μmol), $LiBAr^F_4$ (0.2 μmol), $Ni(COD)_2$ (0.8 μmol). [e]Reaction was run for 30 min.

Ethylene Polymerization. We had demonstrated previously that **Ni3** in combination with $NaBAr^F_4$ was a highly efficient catalyst for ethylene polymerization.[51] To expand our studies to include other alkali ions, we carried out polymerization reactions using both conventional and PEGylated nickel complexes (Table 3). Our standard reactions were conducted in high-pressure reactors using 0.5 μmol nickel complex in 100 mL of toluene under 450 psi of ethylene. The Ni complexes were activated by treatment with $Ni(COD)_2$ (COD = 1,5-cyclooctadiene) as a phosphine scavenger and the reac-

tions were allowed to proceed for 1 h. To establish a baseline for comparison, the mononickel complexes **Ni1** and **Ni2** were tested first. At 30 ˚C, **Ni1** (entry 1) and **Ni2** (entry 2) showed moderate activities of 1.5×10^3 and 2.6×10^3 kg/mol·h, respectively. Because **Ni1** and **Ni2** are similar in their steric bulk ($\%V_{bur}$ = 43.9 and 43.3, respectively), the different rates observed were attributed to differences in their electronic properties (E = +26 mV for **Ni1** vs. -49 mV for **Ni2**). This result is contrary to commonly observed trends that electron-poor catalysts are typically faster than electron-rich ones,[71-73] but is consistent with this family of catalysts.[74] Electron-poor complexes could exhibit longer induction periods due to slower dissociation of the coordinated phosphine. In fact, we found that at 90 ˚C when presumably phosphine abstraction is more facile, the activity of **Ni1** (2.1×10^4 kg/mol·h, entry 16) was similar to that of **Ni2** (2.6×10^4 kg/mol·h, entry 17). The polyethylene (PE) products obtained from both **Ni1** and **Ni2** have low branching (≤ 15 branches/1000 C) and low molecular weight (M_n = ~10^3 g/mol), which are similar to those reported for nickel phenoxyphosphine catalysts.[56]

When **Ni3**/Ni(COD)$_2$ were combined under 450 psi of ethylene, negligible amounts of PE were obtained (Table 3, entry 3). In the absence of alkali ions, the free PEG chain in **Ni3** is believed to be capable of inhibiting the catalyst via nickel coordination. When M^+ was added, the catalyst "switched on" dramatically and large quantities of PE were produced. At 30 ˚C (entries 4-7), the catalyst activities were observed in the order **Ni3**-Li > **Ni3**-Na > **Ni3**-K > **Ni3**-Cs, which tracks with the electron-withdrawing abilities of their M^+ ions.[75] The fastest catalyst **Ni3**-Li (3.5×10^4 kg/mol·h, entry 4) showed 23× and 13× higher activity than that of the mononickel catalysts **Ni1** (entry 1) and **Ni2** (entry 2), respectively. In some reactions, mass transport issues were significant due to the formation of large amounts of insoluble PE.[13]

The PEs obtained from **Ni3**-M showed an inverse relationship between molecular weight and branching (i.e., polymers with higher M_n have fewer branches and vice versa). It is generally found that bulkier catalysts give polymers with higher molecular weight because they could prevent associative chain transfer pathways in favor of chain propagation.[6] Despite not having the largest $\%V_{bur}$ in the series, **Ni3**-Li yielded PE with the highest molecular weight (4.0×10^4 g/mol, Table 3, entry 4). The bulkiest catalyst **Ni3**-Cs afforded PE with only a slightly lower M_n of 3.4×10^4 g/mol (entry 7). To rationalize these results, it should be noted that electronic effects could also lead to enhanced polymer molecular weight if the rate of chain propagation increases more significantly than the rate of chain transfer. In fact, the chain growth rate of **Ni3**-Li was about 20× faster than that of **Ni3**-Cs (assuming they are proportional to their polymer yields of 3.53 and 0.18 g, respectively), but its chain transfer rate was about 16× slower.[76] We cannot compare these rates to those of their parent complex **Ni3** because it is catalytically inactive. In a separate Lewis acid study, Jordan and coworkers found that addition of boranes to Pd catalysts increased chain growth rates by only about 3× but increased chain transfer rates by up to 80×.[77] These changes were attributed to electronic perturbations that placed more partial positive charge at the palladium center. In contrast, because both structural and electronic changes occur in our catalysts as a result of secondary metal binding, both contributions must be considered *together* to fully explain the cation effect.

The **Ni3**-M catalysts produced PEs with branches ranging from 9–27/1000 C, indicating the alkali ions also affected chain-walking processes (i.e., β-hydride elimination/reinsertion) to different degrees. Although nickel catalysts typically furnish polymers with fewer branches than their palladium analogues, which could have as many as 100+ branches/1000 C,[6] our results clearly showed that cation-tuning is a viable strategy to prepare PE with customized morphologies (Scheme 1).

Next, we investigated how various reaction parameters affected polymerization. We observed that the **Ni3**-M catalysts had different optimal temperatures. Using a standard catalyst loading of 0.5 μmol, we found **Ni3**-Li was most active at 50 ˚C, **Ni3**-Na was most active at 30 ˚C, and both **Ni3**-K and **Ni3**-Cs were most active at 70 ˚C (Figure 3A, Table 3). Their PE molecular weights generally decreased, whereas their branching densities were only minimally affected by increasing temperatures (Figure S6).

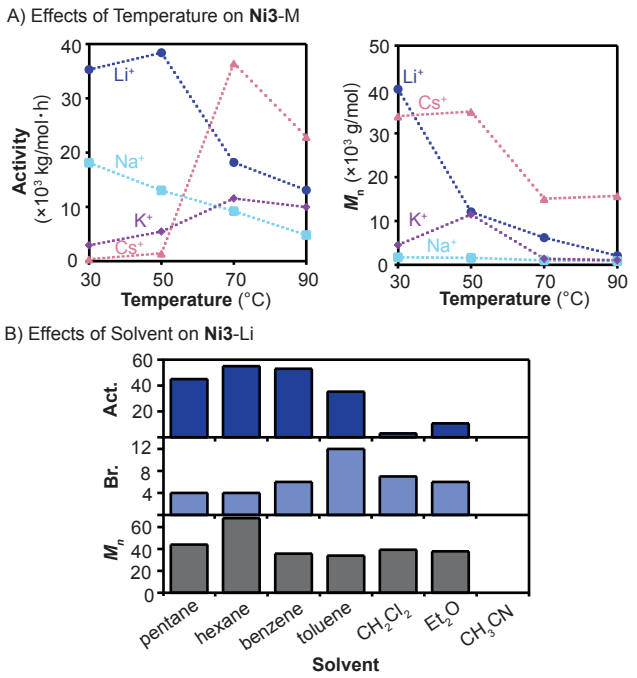

Figure 3. Plots showing A) the effects of temperature on **Ni3**-M (M = Li^+, Na^+, K^+ or Cs^+, see Table 3 for details) and B) the effects of solvent on **Ni3**-Li (30 °C, see Table S7 for details). Abbreviations used: Act. = Activity (×10^3 kg/mol·h), Br. = Branches (/1000 C), M_n = average number molecular weight (×10^3 g/mol).

Surprisingly, **Ni3**-Cs showed impressive catalytic performance even at 90 ˚C (activity = 2.3 ×10^4 kg/mol·h and turnover number or TON = 4.1×10^5 mol ethylene/mol Ni), exceeding that of other thermally stable nickel catalysts reported in the literature (Table S12). For example, the nickel diimine cyclophane catalyst **Ni13** gave lower activity (1.8×10^4 kg/mol·h) and TON (1.6×10^5 mol ethylene/mol Ni) at 90 ˚C.[78] However, catalyst **Ni13** furnished PE with an order of magnitude higher molecular weight (M_n = 2.9 ×10^5 g/mol) than that of **Ni3**-Cs (M_n = 1.6 ×10^4 g/mol). However, in preliminary work we found that our nickel phenoxyphosphine-PEG catalysts could be derivatized with bulkier groups to produce PE with M_n of ~10^6 g/mol so polymer molecular weight is not a

limiting feature of our catalyst. Although **Ni1** and **Ni2** also exhibited high activity at 90 ˚C (~10^4 kg/mol·h), their M_w/M_n increased to ≥ 3.4 (Table 3, entries 16 and 17), suggesting that these complexes were no longer single site catalysts or were decomposing at high temperatures.

The effects of solvent on polymerization were also investigated. In general, **Ni3**-M was more active in non-polar than in polar solvents (Table S5). For example, **Ni3**-Li displayed the highest activity in hexane (5.5×10^4 kg/mol·h) and benzene (5.30×10^4 kg/mol·h) but was completely inhibited in acetonitrile (Figure 3B), probably because the latter could compete with ethylene for catalyst binding. Interestingly, hexane gave PE with the highest molecular weight (6.81×10^4 g/mol) and toluene gave PE with the highest number of branches (12/1000 C) using **Ni3**-Li. As observed in the solid-state structures of **Ni3**-K (Figure S37) and **Ni3**-Cs (Figure S38), the alkali-PEG units are capable of forming solvent adducts, which means the structures of **Ni3**-M might be different in different solvents. The advantage of performing polymerizations in polar solvents, such as ether, is that higher charged cations (e.g., M^{2+} or M^{3+}) could potentially be used as secondary metals.[50]

Because **Ni3**-Li showed the highest activity in our studies, we sought to optimize its reaction conditions even further (Table S6). We found that at 40 °C using a reduced catalyst loading of 0.1 μmol in 200 mL of toluene for 1 h, **Ni3**-Li gave an activity of 7.0×10^4 kg/mol·h (entry 3). Its TON of 2.5×10^6 mol ethylene/mol Ni greatly surpassed that of other highly active nickel ethylene polymerization catalysts reported in the literature (Table S11). For example, the nickel diimine catalyst **Ni4**[79] and nickel tris(adamantyl)phosphine **Ni12**[14] gave TONs of ~4.0×10^5 and 2.2×10^5 mol ethylene/mol Ni, respectively.

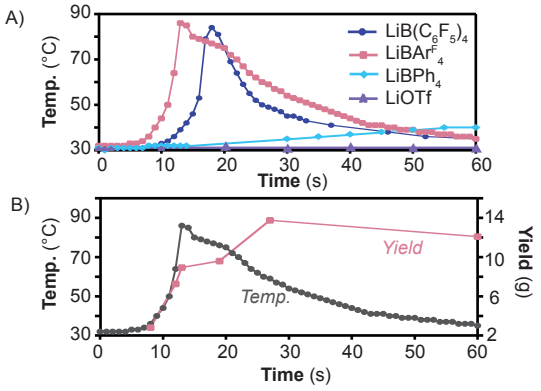

Figure 4. A) Reaction temperatures changes in ethylene polymerization catalyzed by **Ni3**-Li generated from **Ni3** and various lithium salts in toluene. See Table S9 for details. B) Temperature vs. yield plot of ethylene polymerization catalyzed by **Ni3**/$LiBAr^F_4$. See Table S10 for details.

The counteranion also seemed to have significant effects on the performance of **Ni3**-Li. In terms of catalyst activity, the order observed was $BAr^F_4^- > B(C_6F_5)_4^- > BPh_4^- >> OTf^-$ (Table S9). This trend correlated well with their metal coordinating abilities, since tetraarylborates are considered spectator ions[80] whereas triflate is not.[81] Monitoring the temperature profiles of **Ni3** and various lithium salts during polymerization allowed us to differentiate the subtle effects of the anions (Figure 4A). For example, **Ni3**+$LiBAr^F_4$ showed a preactivation period of ~5 min before a large exotherm occurred, which maximized at ~13 min (86 ºC). A time-dependent plot of temperature vs. PE yield for **Ni3**+$LiBAr^F_4$ suggested the catalyst deactivated after ~30 min since no additional polymer was produced (Figure 4B). The temperature profile of **Ni3**+$LiB(C_6F_5)_4$ was similar to that of **Ni3**+$LiBAr^F_4$, except the preactivation period lasted ~10 min before the temperature increased exponentially. Interestingly, **Ni3**+$LiBPh_4$ showed a slow linear increase in temperature up to 40 ºC during the 60 min run. As expected, because **Ni3**+LiOTf was not active in polymerization, this reaction showed no changes in temperature. Although the reasons for the different effects of anions have not been studied in detail, we hypothesize that solubility and metal coordinating ability might be major contributing factors.

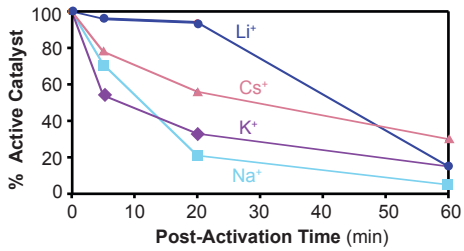

Figure 5. Comparison of **Ni3**-M complexes in ethylene polymerization after various post-activation times. The % active catalyst = [(yield of polymer after x min post-activation)/(yield of polymer after 0 min post-activation)]×100%. See Table S13 for details.

Relative Catalyst Stability. To study the relative stability of the nickel-alkali catalysts, a reactivity-based method was used.[14] The **Ni3**-M complexes were dissolved in 100 mL of toluene/Et_2O (4:1) and then combined with 3 equiv. of $B(C_6F_5)_3$[82] under ~5 psi of ethylene. The reaction mixtures were allowed to stir for various post-activation times and then the ethylene pressure was increased to 450 psi for 1 h (Table S13). The % active catalyst was determined based on the quantity of PE obtained after 5, 20, or 60 min post-activation relative to that of the control with no waiting period. It is important to note these experiments provide only an estimate of the *relative* amounts of active species present rather than the *actual* amounts, which would require more rigorous techniques such as active site labeling.[83,84] A summary of the data is shown in Figure 5. As expected, the amount of PE obtained decreased as the post-activation time increased. After 5 min, ~96, 71, 54, and 78% of active catalysts were observed for **Ni3**-Li, **Ni3**-Na, **Ni3**-K, and **Ni3**-Cs, respectively. The apparent high percentage of **Ni3**-Li calculated (≥ 94% up to 20 min) was not likely due to its greater stability, but rather, to the fact that it is slower to activate than the other **Ni3**-M species (in other words, fresh active species were generated as others decayed). After 60 min, the % active catalyst was observed in the order **Ni3**-Cs > **Ni3**-K ~ **Ni3**-Li > **Ni2**-Na. This experiment most likely overestimates the stability of **Ni3**-Li due to its slower phosphine abstraction rate (vide infra).

Because phosphine abstraction is the first step in catalyst activation, we measured how quickly PMe_3 was removed from the nickel center using ^{31}P NMR spectroscopy. In our reactions, **Ni3** was premixed with $MBAr^F_4$, and then combined with 3 equiv. of $B(C_6F_5)_3$ (Figures S12-S18). The time required for complete consumption of the starting nickel complex was considered the "phosphine abstraction time" (Table 4). We found that at 30 ºC, the initial **Ni3**, **Ni3**-Na, **Ni3**-K, and

Ni3-Cs species disappeared in less than 5 min. Surprisingly, phosphine abstraction from **Ni3**-Li took > 2 h at 30 °C (entry 2) and < 30 min at 50 °C (entry 4). It should be noted that under actual polymerization conditions, this activation step is expected to be much faster because higher ethylene pressure (450 instead of 5 psi) and vigorous stirring are used. When **Ni3** was mixed with $B(C_6F_5)_3$ first and then treated with Li-BAr^F_4, no starting nickel was left after 5 min (entry 3). Because the nickel center in **Ni3**-Li is the most electron-deficient, its Ni–PMe_3 bond is stronger than those in other **Ni3**-M species. Thus, removal of phosphine from **Ni3**-Li is expected to be correspondingly slower.[71]

Table 4. Summary of Phosphine Abstraction Study[a]

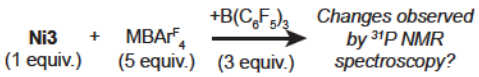

Entry	Complex	Temp. (°C)	Activation Time[b]
1	**Ni3**	30	< 5 min
2	**Ni3**-Li	30	> 2h
3	**Ni3** + ($LiBAr^F_4$)[c]	30	< 5 min
4	**Ni3**-Li	50	< 30 min
5	**Ni3**-Na	30	< 5 min
6	**Ni3**-K	30	< 5 min
7	**Ni3**-Cs	30	< 5 min

[a]Activation study: Complex **Ni3** (7 μmol) and $MBAr^F_4$ (35 μmol, if any) were dissolved in 0.5 mL of toluene-d_8/diethyl ether (4:1) and characterized by ^{31}P NMR spectroscopy. The $B(C_6F_5)_3$ activator (21 μmol) was added and the NMR tube was shaken to mix. [b]The activation time was estimated based on the amount of time it took for the starting complex to convert completely to a new species upon the addition of borane. [c]In this experiment, **Ni3** and $B(C_6F_5)_3$ were combined first to activate the complex before the addition of $LiBAr^F_4$.

Our variable temperature polymerization studies (Figure 3A) and post-activation studies (Figure 5) both support the catalyst stability ranking **Ni3**-Cs > **Ni3**-K > **Ni3**-Li > **Ni2**-Na. Interestingly, this trend correlates well with their $\%V_{bur}$ values (Figure 2), which is reasonable given that greater steric protection should protect the catalysts from undesired decomposition modes. Nickel coordination catalysts are known to degrade through a variety of ways, such as formation of inactive nickel bis(ligand) species or protonolysis of the supporting ligands.[85,86] Since **Ni3**-Cs is the most chemically robust, it is the fastest catalyst at high temperatures (70-90 °C, Table 3). On the other hand, since **Ni3**-Li has the highest intrinsic reactivity, it is the fastest catalyst under conditions in which thermal decay is minimal (e.g., at 30-50 °C). We hypothesize that the short induction period observed during polymerization using **Ni3**-Li (Figure 4) is in part due to slow phosphine abstraction (Table 4).

***Cis*/*Trans* Isomerization and Mechanistic Implications.** Because the solid-state structures showed that both isomers **A** (e.g., **Ni2**, **Ni3**-Li, **Ni3**-K, **Ni3**-Cs) and **B** (e.g., **Ni3**-Na) were isolable, we next investigated their relative distributions in solution. When the ^{31}P NMR spectra of the nickel complexes were recorded in a mixture of toluene-d_8/diethyl ether (4:1) at RT, signals corresponding to the phosphine donors were clearly detected (Figure 6). Because *trans* phosphines (isomer **A**) have larger J_{pp} coupling constants than *cis* phosphines (isomer **B**), isomers **A** and **B** were easily differentiated.[87] The data showed the mononickel complexes all adopted the **A** form in solution. Because **Ni1** is more electron-deficient than **Ni2**, it seems that the electronic nature of nickel *does not* impact its *cis* and *trans* isomer preference (i.e., the *trans* influence is the dominating effect). In fact, there are numerous literature examples of asymmetric square planar nickel complexes that favor having phosphine *trans* to another phosphine rather than to a stronger donor such as alkyl or aryl.[88-91]

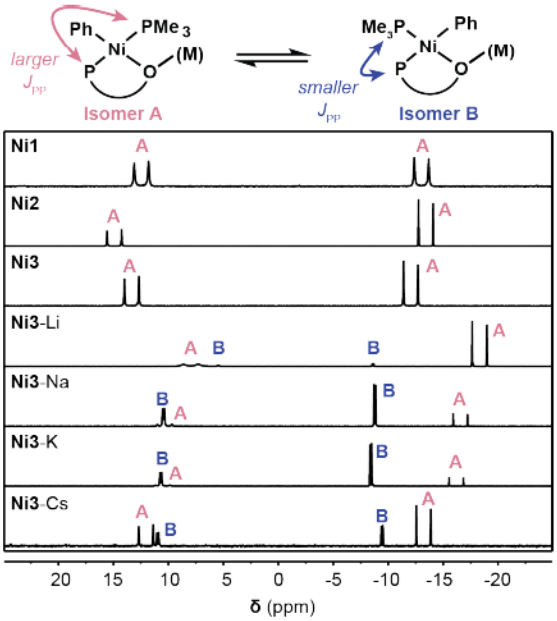

Figure 6. ^{31}P NMR spectra (toluene-d_8/diethyl ether (4:1), 243 MHz) of various nickel complexes showing the equilibrium distribution of isomers **A** and **B** in solution at RT.

Interestingly, **Ni3**-M gave both isomers in various ratios in toluene-d_8/diethyl ether (4:1) (Figure 6). Based on their NMR peak integrations, the equilibrium constants (K_{eq} = [**B**]/[**A**]) were calculated to be 0.1, 9.0, 7.3, and 0.5 for **Ni3**-Li, **Ni3**-Na, **Ni3**-K, and **Ni3**-Cs, respectively. The relatively large amounts of isomer **B** observed in these samples suggest additional forces must be responsible for their greater stability. Based on their K_{eq} values, the free energy change associated with converting isomer **A** to **B** (ΔG_{obs}) was determined to be 1.4, -1.3, -1.2, and 0.4 kcal/mol for **Ni3**-Li, **Ni3**-Na, **Ni3**-K, and **Ni3**-Cs, respectively. Clearly the different alkali ions affect the equilibrium distribution of **A** and **B** differently.

To identify the factors underlying the thermodynamic preference for isomer **A** vs. **B**, we performed density functional theory (DFT) calculations on the nickel complexes. Qualitatively, the calculated results were consistent with our experimental data. We found that ΔG_{calc} for isomerization of **A** to **B** was 9.3, 6.6, and 6.2 kcal/mol for the mononickel complexes **Ni1**, **Ni2**, and **Ni3**, respectively (Table S15), which indicates the equilibrium is strongly in favor of isomer **A**. In contrast, the ΔG_{calc} was 2.0, -2.8, -1.1, and 3.3 kcal/mol for **Ni3**-Li, **Ni3**-Na, **Ni3**-K, and **Ni3**-Cs, respectively. These free energy terms indicate a slight preference of **A** over **B** for **Ni3**-Li and **Ni**-Cs, whereas there is a slight preference of **B** over **A** for

Ni3-Na and **Ni**-K, which was shown by ^{31}P NMR spectroscopic measurements (Figure 6). Although we have confidence in the calculated trends, the accuracy of the ΔG_{calc} values is somewhat limited because we did not include solvent coordination and solvation models in the calculations, which may be different for each complex and would require further experimental studies to guide computational models. The most intriguing result from our DFT studies was that the structures of isomer **B** for **Ni3**-M all showed metal-π interactions between the nickel-coordinated phenyl ring and the neighboring alkali ion (Figure S39). For example, the M(1)–C(30) distances were computed to be 3.27 and 3.22 Å in the optimized **B** structures for **Ni3**-Na and **Ni3**-K, respectively (sum of Van der Waals radii: Na–C = 4.1 Å and K–C = 4.5 Å[92]). These distances were shorter than those in **Ni3**-Li and **Ni3**-Cs, which suggests that Na^+ and K^+ ions have greater π orbital overlap with the phenyl group than Li^+ and Cs^+. It appears that if the stabilization provided by alkali-π interactions exceeds the energy penalty for having unfavorable square planar nickel arrangements, then isomer **B** is thermodynamically accessible.

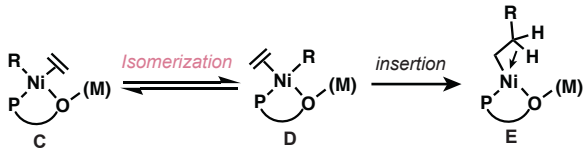

Scheme 3. Proposed pathway for chain propagation involving a key isomerization step from **C** to **D**.

Although the propagating nickel species during polymerization will not have a coordinated phenyl group to participate in alkali-π interactions, the results above led us to wonder whether alkali ions could be involved in *cis*/*trans* isomerization in other ways. In particular, might such behavior account for their polymerization rate enhancing effects? A prevailing mechanistic hypothesis in the literature is that nickel and palladium complexes with asymmetric supporting ligands undergo polymerization mechanisms that alternate between two different geometric isomers.[93,94] For example, it is believed that ethylene coordination to a nickel(*β*-agostic alkyl) complex leads to formation of isomer **C** because it avoids positioning the better phosphine and alkyl donors *trans* to each other (Scheme 3).[95-97] Given that our polymerization data clearly showed significant rate enhancements due to addition of M^+ to **Ni3**, we speculate alkali ions must play integral roles in the reaction beyond just electronic tuning. Although further studies are needed to differentiate between possible isomerization mechanisms,[98-101] such complex undertakings are beyond the scope of this paper. In fact, the tentative nickel(alkyl)(ethylene) species (**C** or **D**) of any catalyst system has not been observed experimentally, presumably due to their extraordinarily reactive nature. Reported studies of such intermediates have been done either computationally[94] or using less reactive palladium analogs.[13] It is entirely possible that *cis*/*trans* isomerization is not responsible for the rate enhancing effects of M^+ but this hypothesis is worthy of further scrutiny. An alternative explanation is that the **Ni3**-M complexes are formally cationic species so their greater charge compared to that of **Ni3** might lead to improved ethylene binding and insertion efficiency.

Conclusion

We have developed a cation-tunable nickel catalyst capable of furnishing polyethylene with distinct morphologies. In previous work, we had encountered design difficulties such as undesirable catalyst bridging,[40] uncontrollable nuclearity,[53] and far nickel-alkali distances.[50] However, we have overcome these synthetic challenges using a nickel phenoxyphosphine-PEG catalyst platform. For the first time, we were able to obtain crystallographic characterization of the complete nickel-alkali series (M = Li^+, Na^+, K^+, and Cs^+), which allowed us to quantify their steric bulk by calculating the percentage buried volumes. The topographic steric maps of **Ni3**-M revealed the complexes not only have greater $\%V_{bur}$ than that of the conventional catalysts **Ni1** and **Ni2** but their alkali-PEG units also protect the nickel axial sites better than pentafluorophenyl or *tert*-butyl groups. Our cyclic voltammetry measurements suggested the alkali ions also decreased the electron density of the nickel complexes, with Li^+ having greater electron-withdrawing capability than even pentafluorophenyl. The impact of alkali ions on polymerization was remarkable as evident by the catalysts' record-breaking performance (quantified by activity and turnover number) and unusual thermal stability. At moderate temperatures (30-50 °C), the activity of **Ni3**-M correlated with the Lewis acidity of M^+ but polymer branching and molecular weight were most likely controlled by both steric and electronic factors. At high temperatures (70-90 °C), the **Ni3**-M complexes with greater steric protection were more active, presumably due to their reduced susceptibility toward decomposition. To explain the rate enhancing effects of alkali ions, we prefer mechanistic models in which M^+ participates directly in polymerization. For example, one possibility is that alkali ions promote isomerization of nickel(alkyl)(ethylene) intermediates from the more to less stable isomer by coordinating to the dissociated phenolate in a three-coordinate transition state. However, this hypothesis still needs to be tested.

Our work on cation-tunable complexes suggests that such systems are much too complicated to fully describe using any single molecular descriptor (e.g., steric or electronic). In fact, some of our observations defy established trends. For example, the addition of borane Lewis acids to conventional catalysts led to significant *decrease* in polymer molecular weight whereas addition of alkali Lewis acids to our tunable catalysts often led to significant *increase* (while also enhancing catalyst activity). Furthermore, secondary metals have other functional properties such as ligand or monomer coordinating ability that could play important roles in catalysis. Despite the complicated nature of secondary metals, we propose that advanced statistical techniques could be used to develop predictive models for guiding cation selection in future polymerization studies.[102]

We anticipate that our cation tuning strategy will allow us to achieve more sophisticated polymer synthesis capabilities. For example, we envision it might be feasible to prepare multi-modal polymers by using two different secondary metals simultaneously or obtain block polymers from a single monomer feed by adding or removing secondary metals in living polymerization reactions. These possibilities suggest that cation-regulated polymerization could be highly versatile and potentially offer improved efficiency and control over existing methods.

Experimental

General Procedures. Commercial reagents were used as received. All air- and water-sensitive manipulations were performed using standard Schlenk techniques or under a nitrogen atmosphere using a drybox. Anhydrous solvents were obtained from an Innovative Technology solvent drying system saturated with argon. High-purity polymer grade ethylene was obtained from Matheson TriGas without further purification. Complexes **Ni2**, **Ni3**, and $NiPhBr(PMe_3)_2$ were prepared according to our previous report.[51] The $LiBAr^F_4$, $NaBAr^F_4$, $KBAr^F_4$ and $CsBAr^F_4$ salts were prepared according to literature procedures.[103,104]

NMR spectra were acquired using JEOL spectrometers (ECA-400, -500, and -600) and referenced using residual solvent peaks. All ^{13}C NMR spectra were proton decoupled. ^{31}P NMR spectra were referenced to phosphoric acid. ^1H NMR spectroscopic characterization of polymers: each NMR sample contained ~20 mg of polymer in 0.5 mL of 1,1,2,2-tetrachloroethane-d_2 (TCE-d_2) and was recorded on a 500 MHz spectrometer using standard acquisition parameters at 120 °C.

Gel permeation chromatography (GPC) data were obtained using a Malvern high temperature GPC instrument equipped with refractive index, viscometer, and light scattering detectors at 150 °C with 1,2,4-trichlorobenzene (stabilized with 125 ppm BHT) as the mobile phase. A calibration curve was established using polystyrene standards in triple detection mode. All molecular weights reported are based on the triple detection method.

General Procedure for Ethylene Polymerization. Inside the drybox, the nickel complex (0.5 μmol) and $MBAr^F_4$ (1 μmol, if any) were dissolved in 10 mL of toluene in a 20 mL vial and stirred for 10 min. Solid $Ni(COD)_2$ (4 μmol) was added and stirred until a clear solution was obtained (4−5 min). The mixture was loaded into a 10 mL syringe equipped with an 8-inch stainless steel needle. The loaded syringe was sealed by sticking the needle tip into a rubber septum and brought outside of the drybox. To prepare the polymerization reactor, 90 mL of dry toluene was placed in an empty autoclave. The autoclave was pressurized with ethylene to 80 psi, stirred for 5 min, and then the reactor pressure was reduced to 5 psi. This process was repeated 3 times to remove trace amounts of oxygen inside the reaction vessel. The reactor was then heated to the desired temperature and the catalyst solution was injected into the autoclave through a side arm. The autoclave was sealed and purged with ethylene at 40 psi (no stirring) three times. Finally, the reactor pressure was increased to the desired pressure, and the contents were stirred vigorously. To stop the polymerization, the autoclave was vented and cooled in an ice bath. A solution of MeOH (700 mL) was added to precipitate the polymer. The polymer was collected by vacuum filtration, rinsed with MeOH, and dried under vacuum at 80 °C overnight. The reported yields are average values obtained from duplicate or triplicate runs. The standard deviations are typically within 7% but no more than 10%.

Computational Methods. All geometries were optimized at B3LYP-D3 using the 6-31G(d) basis set for the H, Li, C, O, F, Na, P and K atoms, and the Lanl2DZ basis set with effective core potential for Ni and Cs, employing the Gaussian16 program. This choice of method and basis set combination has been applied in computational studies of ethylene polymerization as well as other mechanistic studies involving Ni atoms.[94,105] Vibrational frequency analyses verified the nature of the minima and transition state structures. Gas-phase Gibbs free energies were computed at 298.15 K and verified the *cis*/*trans* conformational preferences of the nickel complexes. Three dimensional structures were produced with the CYLView 1.0.1 software.[106]

AUTHOR INFORMATION

Corresponding Author

* Loi H. Do – Department of Chemistry, University of Houston
Orchid ID: https://orcid.org/0000-0002-8859-141X
Email: loido@uh.edu

Notes

The authors declare no competing financial interest.

ASSOCIATED CONTENT

Supporting Information.
Experimental procedures, spectroscopic data, metal binding studies, polymerization data, and DFT calculations. This material is available free of charge via the Internet at http://pubs.acs.org.

ACKNOWLEDGMENT

We are extremely grateful to the Welch Foundation (E-1894 to L.H.D.), the National Science Foundation (CHE-1750411 to L.H.D. and CHE-1751370 to J.I.W.), and the National Institute of General Medical Sciences of the National Institutes of Health (R35GM133548 to J.I.W.) for grant support. We acknowledge the use of the Sabine cluster and support from the Research Computing Data Core at the University of Houston. We thank Prof. Tom Teets for allowing us to use a potentiostat for electrochemical measurements.

REFERENCES

(1) Whiteley, K. S. Polyethylene. In *Ullmann's Encyclopedia of Industrial Chemistry*; Wiley-VCH Verlag GmbH & Co. KGaA: 2012; Vol. 29, p 1-38.
(2) Johnson, L. K.; Killian, C. M.; Brookhart, M. New Pd(II)- and Ni(II)-Based Catalysts for Polymerization of Ethylene and α-Olefins. *J. Am. Chem. Soc.*, **1995**, *117* (23), 6414-6415.
(3) Johnson, L. K.; Mecking, S.; Brookhart, M. Copolymerization of Ethylene and Propylene with Functionalized Vinyl Monomers by Palladium(II) Catalysts. *J. Am. Chem. Soc.*, **1996**, *118* (1), 267-268.
(4) Mitchell, N. E.; Long, B. K. Recent Advances in Thermally Robust, Late Transition Metal-Catalyzed Olefin Polymerization. *Polym. Int.*, **2019**, *68* (1), 14-26.
(5) Chen, C. Designing Catalysts for Olefin Polymerization and Copolymerization: Beyond Electronic and Steric Tuning. *Nat. Rev. Chem.*, **2018**, *2* (5), 6-14.
(6) Guo, L.; Dai, S.; Sui, X.; Chen, C. Palladium and Nickel Catalyzed Chain Walking Olefin Polymerization and Copolymerization. *ACS Catal.*, **2016**, *6* (1), 428-441.
(7) Wang, J.; Wang, L.; Yu, H.; Ullah, R. S.; Haroon, M.; Zain ul, A.; Xia, X.; Khan, R. U. Recent Progress in Ethylene Polymerization Catalyzed by Ni and Pd Catalysts. *Eur. J. Inorg. Chem.*, **2018**, *2018* (13), 1450-1468.
(8) Carrow, B. P.; Nozaki, K. Transition-Metal-Catalyzed Functional Polyolefin Synthesis: Effecting Control Through Chelating Ancillary Ligand Design and Mechanistic Insights. *Macromolecules*, **2014**, *47* (8), 2541-2555.
(9) Nakamura, A.; Ito, S.; Nozaki, K. Coordination-Insertion Copolymerization of Fundamental Polar Monomers. *Chem. Rev.*, **2009**, *109* (11), 5215-5244.
(10) Ittel, S. D.; Johnson, L. K.; Brookhart, M. Late-Metal Catalysts for Ethylene Homo- and Copolymerization. *Chem. Rev.*, **2000**, *100* (4), 1169-1203.

(11) Nakamura, A.; Anselment, T. M. J.; Claverie, J.; Goodall, B.; Jordan, R. F.; Mecking, S.; Rieger, B.; Sen, A.; van Leeuwen, P. W. N. M.; Nozaki, K. Ortho-Phosphinobenzenesulfonate: A Superb Ligand for Palladium-Catalyzed Coordination-Insertion Copolymerization of Polar Vinyl Monomers. *Acc. Chem. Res.*, **2013**, *46* (7), 1438-1449.
(12) Walsh, D. J.; Hyatt, M. G.; Miller, S. A.; Guironnet, D. Recent Trends in Catalytic Polymerizations. *ACS Catal.*, **2019**, 11153-11188.
(13) Tran, Q. H.; Brookhart, M.; Daugulis, O. New Neutral Nickel and Palladium Sandwich Catalysts: Synthesis of Ultra-High Molecular Weight Polyethylene (UHMWPE) via Highly Controlled Polymerization and Mechanistic Studies of Chain Propagation. *J. Am. Chem. Soc.*, **2020**, *142* (15), 7198-7206.
(14) Kocen, A. L.; Brookhart, M.; Daugulis, O. A Highly Active Ni(II)-Triadamantylphosphine Catalyst for Ultrahigh-Molecular-Weight Polyethylene Synthesis. *Nature Commun.*, **2019**, *10* (1), 438.
(15) Kenyon, P.; Wörner, M.; Mecking, S. Controlled Polymerization in Polar Solvents to Ultrahigh Molecular Weight Polyethylene. *J. Am. Chem. Soc.*, **2018**, *140* (21), 6685-6689.
(16) Chen, M.; Chen, C. A Versatile Ligand Platform for Palladium- and Nickel-Catalyzed Ethylene Copolymerization with Polar Monomers. *Angew. Chem., Int. Ed.*, **2018**, *57* (12), 3094-3098.
(17) Zhang, W.; Waddell, P. M.; Tiedemann, M. A.; Padilla, C. E.; Mei, J.; Chen, L.; Carrow, B. P. Electron-Rich Metal Cations Enable Synthesis of High Molecular Weight, Linear Functional Polyethylenes. *J. Am. Chem. Soc.*, **2018**, *140* (28), 8841-8850.
(18) Ota, Y.; Ito, S.; Kuroda, J.-i.; Okumura, Y.; Nozaki, K. Quantification of the Steric Influence of Alkylphosphine–Sulfonate Ligands on Polymerization, Leading to High-Molecular-Weight Copolymers of Ethylene and Polar Monomers. *J. Am. Chem. Soc.*, **2014**, *136* (34), 11898-11901.
(19) Sita, L. R. Ex Uno Plures ("Out of One, Many"): New Paradigms for Expanding the Range of Polyolefins through Reversible Group Transfers. *Angew. Chem., Int. Ed.*, **2009**, *48* (14), 2464-2472.
(20) Alam, M. M.; Jack, K. S.; Hill, D. J. T.; Whittaker, A. K.; Peng, H. Gradient Copolymers – Preparation, Properties and Practice. *Eur. Polym. J.*, **2019**, *116* 394-414.
(21) Arriola, D. J.; Carnahan, E. M.; Hustad, P. D.; Kuhlman, R. L.; Wenzel, T. T. Catalytic Production of Olefin Block Copolymers via Chain Shuttling Polymerization. *Science*, **2006**, *312* (5774), 714.
(22) Padilla-Vélez, O.; O'Connor, K. S.; LaPointe, A. M.; MacMillan, S. N.; Coates, G. W. Switchable Living Nickel(ii) α-Diimine Catalyst for Ethylene Polymerisation. *Chem. Commun.*, **2019**, 7607-7610.
(23) Sifri, R. J.; Padilla-Vélez, O.; Coates, G. W.; Fors, B. P. Controlling the Shape of Molecular Weight Distributions in Coordination Polymerization and Its Impact on Physical Properties. *J. Am. Chem. Soc.*, **2020**, *142* (3), 1443-1448.
(24) Wei, J.; Diaconescu, P. L. Redox-Switchable Ring-Opening Polymerization with Ferrocene Derivatives. *Acc. Chem. Res.*, **2019**, *52* (2), 415-424.
(25) Ihrig, S. P.; Eisenreich, F.; Hecht, S. Photoswitchable Polymerization Catalysis: State of the Art, Challenges, and Perspectives. *Chem. Commun.*, **2019**, *55* (30), 4290-4298.
(26) Chen, C. Redox-Controlled Polymerization and Copolymerization. *ACS Catal.*, **2018**, *8* (6), 5506-5514.
(27) Kaiser, J. M.; Long, B. K. Recent Developments in Redox-Active Olefin Polymerization Catalysts. *Coord. Chem. Rev.*, **2018**, *372* 141-152.
(28) Teator, A. J.; Lastovickova, D. N.; Bielawski, C. W. Switchable Polymerization Catalysts. *Chem. Rev.*, **2016**, *116* (4), 1969-1992.
(29) Biernesser, A. B.; Li, B.; Byers, J. A. Redox-Controlled Polymerization of Lactide Catalyzed by Bis(imino)pyridine Iron Bis(alkoxide) Complexes. *J. Am. Chem. Soc.*, **2013**, *135* (44), 16553-16560.
(30) Biernesser, A. B.; Delle Chiaie, K. R.; Curley, J. B.; Byers, J. A. Block Copolymerization of Lactide and an Epoxide Facilitated by a Redox Switchable Iron-Based Catalyst. *Angew. Chem., Int. Ed.*, **2016**, *55* (17), 5251-5254.
(31) The term "switchable catalyst" has also been used to describe such complexes. However, not all tunable catalysts have been demonstrated to have switching capability, which implies the ability to toggle between different reactivity states during catalysis.
(32) Chen, M.; Yang, B.; Chen, C. Redox-Controlled Olefin (Co)Polymerization Catalyzed by Ferrocene-Bridged Phosphine-Sulfonate Palladium Complexes. *Angew. Chem., Int. Ed.*, **2015**, *54* (51), 15520-15524.
(33) Zhao, M.; Chen, C. Accessing Multiple Catalytically Active States in Redox-Controlled Olefin Polymerization. *ACS Catal.*, **2017**, *7* (11), 7490-7494.
(34) Anderson, W. C.; Park, S. H.; Brown, L. A.; Kaiser, J. M.; Long, B. K. Accessing Multiple Polyethylene Grades via a Single Redox-Active Olefin Polymerization Catalyst. *Inorg. Chem. Front.*, **2017**, *4* (7), 1108-1112.
(35) Anderson, W. C.; Long, B. K. Modulating Polyolefin Copolymer Composition via Redox-Active Olefin Polymerization Catalysts. *ACS Macro Lett.*, **2016**, *5* (9), 1029-1033.
(36) Kaiser, J. M.; Anderson, W. C.; Long, B. K. Photochemical Regulation of a Redox-Active Olefin Polymerization Catalyst: Controlling Polyethylene Microstructure with Visible Light. *Polym. Chem.*, **2018**, *9* (13), 1567-1570.
(37) Keyes, A.; Basbug Alhan, H. E.; Ha, U.; Liu, Y.-S.; Smith, S. K.; Teets, T. S.; Beezer, D. B.; Harth, E. Light as a Catalytic Switch for Block Copolymer Architectures: Metal–Organic Insertion/Light Initiated Radical (MILRad) Polymerization. *Macromolecules*, **2018**, *51* (18), 7224-7232.
(38) Keyes, A.; Dau, H.; Basbug Alhan, H. E.; Ha, U.; Ordonez, E.; Jones, G. R.; Liu, Y.-S.; Tsogtgerel, E.; Loftin, B.; Wen, Z.; Wu, J. I.; Beezer, D. B.; Harth, E. Metal–Organic Insertion Light Initiated Radical (MILRad) Polymerization: Photo-Initiated Radical Polymerization of Vinyl Polar Monomers with Various Palladium Diimine Catalysts. *Polym. Chem.*, **2019**, *10* (23), 3040-3047.
(39) Johnson, L.; Wang, L.; McLain, S.; Bennett, A.; Dobbs, K.; Hauptman, E.; Ionkin, A.; Ittel, S.; Kunitsky, K.; Marshall, W.; McCord, E.; Radzewich, C.; Rinehart, A.; Sweetman, K. J.; Wang, Y.; Yin, Z.; Brookhart, M. Copolymerization of Ethylene and Acrylates by Nickel Catalysts. In *Beyond Metallocenes*; American Chemical Society: 2003; Vol. 857, p 131-142.
(40) Cai, Z.; Xiao, D.; Do, L. H. Fine-Tuning Nickel Phenoxyimine Olefin Polymerization Catalysts: Performance Boosting by Alkali Cations. *J. Am. Chem. Soc.*, **2015**, *137* (49), 15501-15510.
(41) Cai, Z.; Do, L. H. Customizing Polyolefin Morphology by Selective Pairing of Alkali Ions with Nickel Phenoxyimine-Polyethylene Glycol Catalysts. *Organometallics*, **2017**, *36* (24), 4691-4698.
(42) Chiu, H.-C.; Pearce, A. J.; Dunn, P. L.; Cramer, C. J.; Tonks, I. A. β-Oxo-δ-diimine Nickel Complexes: A Comparison of Tautomeric Active Species in Ethylene Polymerization Catalysis. *Organometallics*, **2016**, *35* (12), 2076-2085.
(43) Cai, Z.; Xiao, D.; Do, L. H. Cooperative Heterobimetallic Catalysts in Coordination Insertion Polymerization. *Comments Inorg. Chem.*, **2019**, *39* (1), 27-50.
(44) Liu, Q.; Jordan, R. F. Sterically Controlled Self-Assembly of a Robust Multinuclear Palladium Catalyst for Ethylene Polymerization. *J. Am. Chem. Soc.*, **2019**, *141* (17), 6827-6831.
(45) Shen, Z.; Jordan, R. F. Copolymerization of Ethylene and Vinyl Fluoride by (Phosphine-bis(arenesulfonate))PdMe(pyridine) Catalysts: Insights into Inhibition Mechanisms. *Macromolecules*, **2010**, *43* (21), 8706-8708.
(46) Shen, Z.; Jordan, R. F. Self-Assembled Tetranuclear Palladium Catalysts That Produce High Molecular Weight Linear Polyethylene. *J. Am. Chem. Soc.*, **2010**, *132* (1), 52-53.
(47) Wei, J.; Shen, Z.; Filatov, A. S.; Liu, Q.; Jordan, R. F. Self-Assembled Cage Structures and Ethylene Polymerization Behavior of Palladium Alkyl Complexes That Contain

Phosphine-Bis(arenesulfonate) Ligands. *Organometallics*, **2016**, *35* (20), 3557-3568.
(48) Liu, Q.; Jordan, R. F. Multinuclear Palladium Olefin Polymerization Catalysts Based on Self-Assembled Zinc Phosphonate Cages. *Organometallics*, **2018**, *37* (24), 4664-4674.
(49) Cai, Z.; Do, L. H. Thermally Robust Heterobimetallic Palladium–Alkali Catalysts for Ethylene and Alkyl Acrylate Copolymerization. *Organometallics*, **2018**, *37* (21), 3874-3882.
(50) Xiao, D.; Cai, Z.; Do, L. H. Accelerating Ethylene Polymerization Using Secondary Metal Ions in Tetrahydrofuran. *Dalton Trans.*, **2019**, *48* (48), 17887-17897.
(51) Tran, T. V.; Nguyen, Y. H.; Do, L. H. Development of Highly Productive Nickel–Sodium Phenoxyphosphine Ethylene Polymerization Catalysts and their Reaction Temperature Profiles. *Polym. Chem.*, **2019**, *10* (27), 3718-3721.
(52) Zhang, D.; Chen, C. Influence of Polyethylene Glycol Unit on Palladium- and Nickel-Catalyzed Ethylene Polymerization and Copolymerization. *Angew. Chem., Int. Ed.*, **2017**, *56* (46), 14672-14676.
(53) Xiao, D.; Do, L. H. In Situ Generated Heterometallic Nickel–Zinc Catalysts for Ethylene Polymerization. *Organometallics*, **2018**, *37* (18), 3079-3085.
(54) Xin, B. S.; Sato, N.; Tanna, A.; Oishi, Y.; Konishi, Y.; Shimizu, F. Nickel Catalyzed Copolymerization of Ethylene and Alkyl Acrylates. *J. Am. Chem. Soc.*, **2017**, *139* (10), 3611-3614.
(55) Zhang, Y.; Mu, H.; Pan, L.; Wang, X.; Li, Y. Robust Bulky [P,O] Neutral Nickel Catalysts for Copolymerization of Ethylene with Polar Vinyl Monomers. *ACS Catal.*, **2018**, *8* 5963-5976.
(56) Zhang, Y.-P.; Li, W.-W.; Li, B.-X.; Mu, H.-L.; Li, Y.-S. Well-Defined Phosphino-Phenolate Neutral Nickel(II) Catalysts for Efficient (Co)polymerization of Norbornene and Ethylene. *Dalton Trans.*, **2015**, *44* (16), 7382-7394.
(57) Renny, J. S.; Tomasevich, L. L.; Tallmadge, E. H.; Collum, D. B. Method of Continuous Variations: Applications of Job Plots to the Study of Molecular Associations in Organometallic Chemistry. *Angew. Chem., Int. Ed.*, **2013**, *52* (46), 11998-12013.
(58) Bogan, M. J.; Agnes, G. R. Poly(ethylene glycol) Doubly and Singly Cationized by Different Alkali Metal Ions: Relative Cation Affinities and Cation-Dependent Resolution in a Quadrupole Ion Trap Mass Spectrometer. *J. Am. Soc. Mass Spectrom.*, **2002**, *13* (2), 177-186.
(59) Tsuda, A.; Fukumoto, C.; Oshima, T. Self-Activated Supramolecular Reactions: Effects of Host−Guest Recognition on the Kinetics of the Diels−Alder Reaction of Open-Chain Oligoether Quinones With Cyclopentadiene. *J. Am. Chem. Soc.*, **2003**, *125* (19), 5811-5822.
(60) Appleton, T. G.; Clark, H. C.; Manzer, L. E. The *trans*-Influence: Its Measurement and Significance. *Coord. Chem. Rev.*, **1973**, *10* (3), 335-422.
(61) Rezabal, E.; Ugalde, J. M.; Frenking, G. The *trans* Effect in Palladium Phosphine Sulfonate Complexes. *J. Phys. Chem. A*, **2017**, *121* (40), 7709-7716.
(62) Gokel, G. W.; Barbour, L. J.; Ferdani, R.; Hu, J. Lariat Ether Receptor Systems Show Experimental Evidence for Alkali Metal Cation−π Interactions. *Acc. Chem. Res.*, **2002**, *35* (10), 878-886.
(63) Shannon, R. Revised Effective Ionic Radii and Systematic Studies of Interatomic Distances in Halides and Chalcogenides. *Acta Cryst. A*, **1976**, *32* (5), 751-767.
(64) Falivene, L.; Credendino, R.; Poater, A.; Petta, A.; Serra, L.; Oliva, R.; Scarano, V.; Cavallo, L. SambVca 2. A Web Tool for Analyzing Catalytic Pockets with Topographic Steric Maps. *Organometallics*, **2016**, *35* (13), 2286-2293.
(65) Falivene, L.; Cao, Z.; Petta, A.; Serra, L.; Poater, A.; Oliva, R.; Scarano, V.; Cavallo, L. Towards the Online Computer-Aided Design of Catalytic Pockets. *Nat. Chem.*, **2019**, *11* (10), 872-879.
(66) Gong, Y.; Li, S.; Gong, Q.; Zhang, S.; Liu, B.; Dai, S. Systematic Investigations of Ligand Steric Effects on α-Diimine Nickel Catalyzed Olefin Polymerization and Copolymerization. *Organometallics*, **2019**, *38* (15), 2919-2926.
(67) Sun, J.; Chen, M.; Luo, G.; Chen, C.; Luo, Y. Diphosphazane-monoxide and Phosphine-sulfonate Palladium Catalyzed Ethylene Copolymerization with Polar Monomers: A Computational Study. *Organometallics*, **2019**, *38* (3), 638-646.
(68) Losada, J.; del Peso, I.; Beyer, L. Redox and Electrocatalytic Properties of Electrodes Modified by Films of Polypyrrole Nickel(II) Schiff-Base Complexes. *J. Electroanal. Chem.*, **1998**, *447* (1), 147-154.
(69) Santos, I. C.; Vilas-Boas, M.; Piedade, M. F. M.; Freire, C.; Duarte, M. T.; de Castro, B. Electrochemical and X-ray Studies of Nickel(II) Schiff Base Complexes Derived from Salicylaldehyde: Structural Effects of Bridge Substituents on the Stabilisation of the +3 Oxidation State. *Polyhedron*, **2000**, *19* (6), 655-664.
(70) Reath, A. H.; Ziller, J. W.; Tsay, C.; Ryan, A. J.; Yang, J. Y. Redox Potential and Electronic Structure Effects of Proximal Nonredox Active Cations in Cobalt Schiff Base Complexes. *Inorg. Chem.*, **2017**, *56* (6), 3713-3718.
(71) Wang, C.; Friedrich, S.; Younkin, T. R.; Li, R. T.; Grubbs, R. H.; Bansleben, D. A.; Day, M. W. Neutral Nickel(II)-Based Catalysts for Ethylene Polymerization. *Organometallics*, **1998**, *17* (15), 3149-3151.
(72) Li, S.; Xu, G.; Dai, S. A Remote Nonconjugated Electron Effect in Insertion Polymerization with α-Diimine Nickel and Palladium Species. *Polym. Chem.*, **2020**, *11* (15), 2692-2699.
(73) Kuhn, P.; Sémeril, D.; Matt, D.; Chetcuti, M. J.; Lutz, P. Structure–Reactivity Relationships in SHOP-Type Complexes: Tunable Catalysts for the Oligomerisation and Polymerisation of Ethylene. *Dalton Trans.*, **2007**, (5), 515-528.
(74) Zhang, Y.; Mu, H.; Wang, X.; Pan, L.; Li, Y. Elaborate Tuning in Ligand Makes a Big Difference in Catalytic Performance: Bulky Nickel Catalysts for (Co)polymerization of Ethylene with Promising Vinyl Polar Monomers. *ChemCatChem*, **2019**, *11* (9), 2329-2340.
(75) Brown, I. D.; Skowron, A. Electronegativity and Lewis Acid Strength. *J. Am. Chem. Soc.*, **1990**, *112* (9), 3401-3403.
(76) The rate of chain transfer ($R_{transfer}$) was estimated based on the number average degree of polymerization ($X_n \approx M_n$) and growth rate ($R_{growth} \approx$ polymer yield) using the equation $[R_{transfer,Li}]/[R_{transfer,Cs}] = [X_{Cs}*R_{growth,Li}]/[X_{Li}*R_{growth,Cs}]$. See reference #77 for details.
(77) Cai, Z.; Shen, Z.; Zhou, X.; Jordan, R. F. Enhancement of Chain Growth and Chain Transfer Rates in Ethylene Polymerization by (Phosphine-sulfonate)PdMe Catalysts by Binding of B(C6F5)3 to the Sulfonate Group. *ACS Catal.*, **2012**, *2* (6), 1187-1195.
(78) Camacho, D. H.; Salo, E. V.; Ziller, J. W.; Guan, Z. Cyclophane-Based Highly Active Late-Transition-Metal Catalysts for Ethylene Polymerization. *Angew. Chem., Int. Ed.*, **2004**, *43* (14), 1821-1825.
(79) Gates, D. P.; Svejda, S. A.; Oñate, E.; Killian, C. M.; Johnson, L. K.; White, P. S.; Brookhart, M. Synthesis of Branched Polyethylene Using (α-Diimine)nickel(II) Catalysts: Influence of Temperature, Ethylene Pressure, and Ligand Structure on Polymer Properties. *Macromolecules*, **2000**, *33* (7), 2320-2334.
(80) Krossing, I.; Raabe, I. Noncoordinating Anions—Fact or Fiction? A Survey of Likely Candidates. *Angew. Chem., Int. Ed.*, **2004**, *43* (16), 2066-2090.
(81) Hayashida, T.; Kondo, H.; Terasawa, J.-i.; Kirchner, K.; Sunada, Y.; Nagashima, H. Trifluoromethanesulfonate (Triflate) as a Moderately Coordinating Anion: Studies from Chemistry of the Cationic Coordinatively Unsaturated Mono- and Diruthenium Amidinates. *J. Organomet. Chem.*, **2007**, *692* (1), 382-394.
(82) $B(C_6F_5)_3$ was used as a phosphine scavenger instead of $Ni(COD)_2$ here because it does not generate any insoluble byproducts, which is imporatnt for the spectroscopic studies described below.
(83) Nelsen, D. L.; Anding, B. J.; Sawicki, J. L.; Christianson, M. D.; Arriola, D. J.; Landis, C. R. Chromophore Quench-Labeling: An Approach to Quantifying Catalyst Speciation As Demonstrated for (EBI)$ZrMe_2$/$B(C_6F_5)_3$-Catalyzed

Polymerization of 1-Hexene. *ACS Catal.*, **2016**, *6* (11), 7398-7408.
(84) Desert, X.; Carpentier, J.-F.; Kirillov, E. Quantification of Active Sites in Single-Site Group 4 Metal Olefin Polymerization Catalysis. *Coord. Chem. Rev.*, **2019**, *386* 50-68.
(85) Waltman, A. W.; Younkin, T. R.; Grubbs, R. H. Insights into the Deactivation of Neutral Nickel Ethylene Polymerization Catalysts in the Presence of Functionalized Olefins. *Organometallics*, **2004**, *23* (22), 5121-5123.
(86) Berkefeld, A.; Mecking, S. Deactivation Pathways of Neutral Ni(II) Polymerization Catalysts. *J. Am. Chem. Soc.*, **2009**, *131* (4), 1565-1574.
(87) Ogilvie, F. B.; Jenkins, J. M.; Verkade, J. G. ^{31}P-^{31}P Spin-Spin Coupling in Complexes Containing Two Phosphorus Ligands. *J. Am. Chem. Soc.*, **1970**, *92* (7), 1916-1923.
(88) Konishi, Y.; Tao, W.-j.; Yasuda, H.; Ito, S.; Oishi, Y.; Ohtaki, H.; Tanna, A.; Tayano, T.; Nozaki, K. Nickel-Catalyzed Propylene/Polar Monomer Copolymerization. *ACS Macro Lett.*, **2018**, *7* (2), 213-217.
(89) Keim, W.; Kowaldt, F. H.; Goddard, R.; Krüger, C. Novel Coordination of (Benzoylmethylene)triphenylphosphorane in a Nickel Oligomerization Catalyst. *Angew. Chem., Int. Ed.*, **1978**, *17* (6), 466-467.
(90) Wang, H.-Y.; Jin, G.-X. Highly Active Neutral Nickel(II) Complexes Bearing P,N-Chelate Ligands: Synthesis, Characterization and Their Application to Addition Polymerization of Norbornene. *Eur. J. Inorg. Chem.*, **2005**, *2005* (9), 1665-1670.
(91) Wan, D.-W.; Gao, Y.-S.; Li, J.-F.; Shen, Q.; Sun, X.-L.; Tang, Y. Synthesis, Structure, and Ethylene Polymerization Behavior of Nickel Complexes Based on Benzoylmethylenetri(2-alkoxylphenyl)phosphorane. *Dalton Trans.*, **2012**, *41* (15), 4552-4557.
(92) Batsanov, S. S. Van der Waals Radii of Elements. *Inorg. Mater.*, **2001**, *37* (9), 871-885.
(93) Noda, S.; Nakamura, A.; Kochi, T.; Chung, L. W.; Morokuma, K.; Nozaki, K. Mechanistic Studies on the Formation of Linear Polyethylene Chain Catalyzed by Palladium Phosphine–Sulfonate Complexes: Experiment and Theoretical Studies. *J. Am. Chem. Soc.*, **2009**, *131* (39), 14088-14100.
(94) Nakano, R.; Chung, L. W.; Watanabe, Y.; Okuno, Y.; Okumura, Y.; Ito, S.; Morokuma, K.; Nozaki, K. Elucidating the Key Role of Phosphine–Sulfonate Ligands in Palladium-Catalyzed Ethylene Polymerization: Effect of Ligand Structure on the Molecular Weight and Linearity of Polyethylene. *ACS Catal.*, **2016**, *6* (9), 6101-6113.
(95) Chan, M. S. W.; Deng, L.; Ziegler, T. Density Functional Study of Neutral Salicylaldiminato Nickel(II) Complexes as Olefin Polymerization Catalysts. *Organometallics*, **2000**, *19* (14), 2741-2750.
(96) Michalak, A.; Ziegler, T. Polymerization of Ethylene Catalyzed by a Nickel(+2) Anilinotropone-Based Catalyst: DFT and Stochastic Studies on the Elementary Reactions and the Mechanism of Polyethylene Branching. *Organometallics*, **2003**, *22* (10), 2069-2079.
(97) Zeller, A.; Strassner, T. The Mechanism of Ethylene Polymerization by Nickel Salicylaldiminato Catalysts – Agostic Interactions and their Kinetic Isotope Effects. *J. Organomet. Chem.*, **2006**, *691* (21), 4379-4385.
(98) Zhou, X.; Jordan, R. F. Synthesis, cis/trans Isomerization, and Reactivity of Palladium Alkyl Complexes That Contain a Chelating N-Heterocyclic-Carbene Sulfonate Ligand. *Organometallics*, **2011**, *30* (17), 4632-4642.
(99) Akita, S.; Nakano, R.; Ito, S.; Nozaki, K. Synthesis and Reactivity of Methylpalladium Complexes Bearing a Partially Saturated IzQO Ligand. *Organometallics*, **2018**, *37* (14), 2286-2296.
(100) Zheng, F.; Hutton, A. T.; van Sittert, C. G. C. E.; Moss, J. R.; Mapolie, S. F. Synthesis, Structural Characterization and *cis–trans* Isomerization of Novel (Salicylaldiminato)platinum(ii) Complexes. *Dalton Trans.*, **2013**, *42* (31), 11163-11179.
(101) Zhou, X.; Lau, K.-C.; Petro, B. J.; Jordan, R. F. *cis*/*trans* Isomerization of *o*-Phosphino-Arenesulfonate Palladium Methyl Complexes. *Organometallics*, **2014**, *33* (24), 7209-7214.
(102) Maldonado, A. G.; Rothenberg, G. Predictive Modeling in Homogeneous Catalysis: a Tutorial. *Chem. Soc. Rev.*, **2010**, *39* (6), 1891-1902.
(103) Brookhart, M.; Grant, B.; Volpe, A. F., Jr. [(3,5-$(CF_3)_2C_6H_3)_4B$]-[$H(OEt_2)_2$]·: A Convenient Reagent for Generation and Stabilization of Cationic, Highly Electrophilic Organometallic Complexes. *Organometallics*, **1992**, *11* (11), 3920-3922.
(104) Carreras, L.; Rovira, L.; Vaquero, M.; Mon, I.; Martin, E.; Benet-Buchholz, J.; Vidal-Ferran, A. Syntheses, Characterisation and Solid-State Study of Alkali and Ammonium BArF Salts. *RSC Adv.*, **2017**, *7* (52), 32833-32841.
(105) McCarren, P. R.; Liu, P.; Cheong, P. H.-Y.; Jamison, T. F.; Houk, K. N. Mechanism and Transition-State Structures for Nickel-Catalyzed Reductive Alkyne–Aldehyde Coupling Reactions. *J. Am. Chem. Soc.*, **2009**, *131* (19), 6654-6655.
(106) Legault, C. Y.; CYLview. http:/http://www.cylview.org (accessed on May 1, 2020).

Table of Contents Artwork